

Andreev bound states in Josephson junctions of semi-Dirac semimetals

Ipsita Mandal

*Department of Physics, Shiv Nadar Institution of Eminence (SNIOE),
Gautam Buddha Nagar, Uttar Pradesh 201314, India*

We consider a Josephson junction built with the two-dimensional semi-Dirac semimetal, which features a hybrid of linear and quadratic dispersion around a nodal point. We model the weak link between the two superconducting regions by a Dirac delta potential because it mimics the thin-barrier limit of a superconductor-barrier-superconductor configuration. Assuming a homogeneous pairing in each region, we set up the BdG formalism for electronlike and holelike quasiparticles propagating along the quadratic-in-momentum dispersion direction. This allows us to compute the discrete bound-state energy spectrum ε of the subgap Andreev states localized at the junction. In contrast with the Josephson effect investigated for propagation along linearly dispersing directions, we find a pair of doubly degenerate Andreev bound states. Using the dependence of ε on the superconducting phase difference ϕ , we compute the variation of Josephson current as a function of ϕ .

CONTENTS

I. Introduction	1
II. Semi-Dirac semimetal	2
III. Josephson junction	3
IV. Results	5
V. Summary and outlook	6
References	7

I. INTRODUCTION

In a configuration consisting of two superconductors coupled together by a weak link between them, a dissipationless current flows across the junction in equilibrium [1–3], which is dubbed as the *Josephson current* I_J . I_J is a single-valued and 2π -periodic function the phase difference ϕ of the pair potential in the two superconductors. In such a set-up, the Andreev surface states of the two superconductors hybridize to form Andreev bound states (ABSs) at the junction. These states are the dominant contributors to the Josephson current through the junction [4–6], because the contributions from the excited states in the continuum are negligible. There is an extensive literature devoted to the study of such Josephson effects in two-dimensional (2d) and three-dimensional (3d) materials like graphene and Weyl-like semimetals [5, 7–13], where the weak link is a tunneling barrier. In other words, the two superconducting regions (abbreviated by “S”) are weakly coupled by a middle region consisting of the normal (i.e., non-superconducting) phase (abbreviated by “N”) of a semimetal. Two alternate configurations include S-N-S [5, 7] and S-B-S (where “B” indicates a potential barrier in the N region) [8, 9, 11–13] junctions. While the superconductivity is induced via proximity-effect by placing a conventional s-wave superconductor on top of the corresponding electrode [14], the tunnel barrier can be created by applying a gate voltage V_0 across N. A schematic representation of the S-B-S set-up is illustrated in Fig. 1(a).

The characterization of the Josephson junctions in the Dirac/Weyl-like systems described above has spanned both isotropic and anisotropic bandstructures. For the anisotropic cases, in addition to a linear-in-momentum dispersion along one of the momentum axes (let us call it k_z), there exists quadratic(cubic)-in-momentum variations along the remaining axes orthogonal to k_z [11, 12]. However, in such studies, the propagation direction has always been chosen to be along the linear-in-momentum dispersion axis. To fill in this gap, we consider here a 2d semi-Dirac semimetal, which features a quadratic dispersion along the axis perpendicular to z , which we label as the k_x -axis, and consider the propagation of the quasiparticles/quasiholes along the quadratic dispersion direction. Such hybrid dispersion characteristics appear in the low-energy spectra of a tight-binding model on the (1) honeycomb lattice in a magnetic field (resulting in the so-called Hofstadter spectrum) [15] and (2) square-lattice with three bands of spinless fermions [16]. The 2d anisotropic semimetallic bandstructure can be found in systems like multi-layer VO_2 - TiO_3 nanostructures [16–19], organic conductor α -(BEDT-TTF) $_2\text{I}_3$ [20, 21], deformed graphene [22–25], and cold atoms trapped in an optical honeycomb lattice [26]. The anisotropic nature of the spectrum manifests itself through distinctive signatures in various transport and thermodynamic properties [17, 27–29].

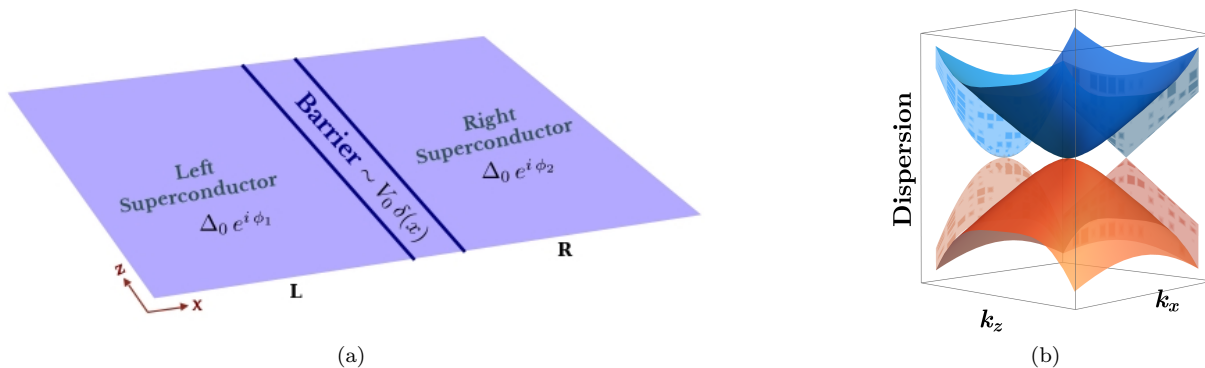


FIG. 1. Schematics of the (a) S-B-S junction configuration; (b) anisotropic dispersion of a semi-Dirac semimetal with a quadratic(linear)-in-momentum dependence along the $k_x(k_z)$ direction. The projections of the dispersion shown in the background clearly demonstrate the hybrid nature.

In this paper, we consider the S-B-S configuration in the thin-barrier limit, constructed with the semi-Dirac semimetal, by approximating the barrier by a Dirac delta function [6, 30, 31]. In our set-up, the weak link is represented by the thin-barrier limit of an S-B-S junction, which is defined by $L \ll \xi$, where L is the barrier thickness and ξ is the superconducting coherence length. We employ the scattering matrix approach for the associated Bogoliubov–de Gennes (BdG) Hamiltonian, which has been one of the standard techniques used extensively to determine the conductance of an N-S junction [32–36], with the appropriate generalization applicable for the S-B-S junctions.

The propagation direction of the quasiparticles/quasiholes is taken to be parallel/antiparallel to the x -axis. We denote the transverse dimension of the junction by W , where W is assumed to be large enough to impose periodic boundary conditions along the z -direction. In the short-barrier regime, the main contribution to the Josephson current comes from the subgap Andreev states [4–6], because the contributions from the excited states in the continuum are suppressed by a factor of L/ξ . We compute the energies of the ABSs in the thin-barrier-limit and determine the resulting the Josephson current.

The paper is organized as follows. In Sec. II, we describe the low-energy effective Hamiltonian of the semi-Dirac semimetal in the normal phase, and show its eigenvalues and eigenfunctions. In Sec. III, the BdG Hamiltonian necessary to describe the S-B-S junction is shown, along with the expressions for electronlike and holelike wavefunctions. This is followed by Sec. IV, where the ABS energy values are derived and the Josephson current is computed numerically. Finally, we end with a summary and outlook in Sec. V.

II. SEMI-DIRAC SEMIMETAL

An effective low-energy continuum model of the 2d anisotropic semi-Dirac semimetal, featuring a hybrid dispersion spectrum which is linear along k_z and quadratic along k_x , is represented by the Hamiltonian [15–19, 27–29, 37]

$$\mathcal{H}(\mathbf{k}) = \frac{\hbar^2 k_x^2}{2m} \sigma_x + \hbar v k_z \sigma_z, \quad (1)$$

where m is the effective mass parameter along the x -axis, v is the Fermi velocity along the z -axis, and σ_x and σ_z are two of the three Pauli matrices. In order to simplify the notations, we define the dimensionless momenta

$$K_x = \frac{\hbar k_x}{p} \text{ and } K_z = \frac{\hbar k_z}{p}, \text{ where } p = 2m v. \quad (2)$$

The tight-binding Hamiltonian [15], from which the above low-energy continuum Hamiltonian has been obtained, consists of a honeycomb lattice comprising two sublattice sites labelled as A and B (analogous to the case for graphene). Hence, there exists a pair of valleys (at the \mathbf{K} and \mathbf{K}' corners of the Brillouin zone) with opposite chiralities, with $\mathcal{H}(\mathbf{k})$ representing the states in the vicinity of the valley with positive chirality (i.e., \mathbf{K} point of the Brillouin zone).

The energy eigenvalues are then given by

$$\mathcal{E} = s \varepsilon_0 \sqrt{K_x^4 + K_z^2}, \quad \varepsilon_0 = \frac{p^2}{2m} = 2p v, \quad s = \pm, \quad (3)$$

as shown in Fig. 1(b). Here the “+” and “−” signs, as usual, refer to the conduction band (i.e., upper band with positive energy eigenvalue) and valence band (i.e., lower band with negative energy eigenvalue), respectively. Henceforth, we set

ε_0 to unity for uncluttering of notations, which just implies that all our energies are scaled in units of ε_0 . Furthermore, we will take $\hbar = 1$ except occasionally for clarity.

The set of two orthonormal eigenvectors is given by

$$\Psi^s(\mathbf{k}) = \frac{1}{\sqrt{K_x^4 + (sE + K_z)^2}} [sE + K_z \quad K_x^2]^T, \quad E = \sqrt{K_x^4 + K_z^2}. \quad (4)$$

In addition to the propagating plane wave solutions, there are also evanescent waves [16, 38–40] present because of the fact that, for a given value of the transverse (to the propagation direction) momentum K_z with $|K_z| \leq |E|$, the relation $K_x^4 = E^2 - K_z^2$ leads to the four solutions $K_x = \pm \mathcal{K}_x$ and $K_x = \pm \tilde{\mathcal{K}}_x$, where $\mathcal{K}_x = (E^2 - K_z^2)^{1/4}$ and $\tilde{\mathcal{K}}_x = i\mathcal{K}_x$. If the Fermi energy cuts the bands at energy E , then for propagation along the x -direction, the corresponding “right-moving” plane waves will have the factor $e^{i \operatorname{sgn}(E) \tilde{\mathcal{K}}_x x}$ — this just implies that if the propagating quasiparticles are occupying the upper(lower) band, then they have a positive(negative) group velocity.

We note that the “extra” solutions involving the evanescent waves (for example, the ones with momentum $\pm \tilde{\mathcal{K}}_x$) do not exist when the propagation direction is taken to be along the z -axis, as the dispersion is linear-in-momentum along that direction. As a result, we expect a richer structure of the ABSs when we analyze the problem of junctions encountered for transmission along the x -direction, which features a nonlinear dependence on the momentum.

III. JOSEPHSON JUNCTION

In order to represent the superconducting phases of the Josephson junction [cf. Fig. 1(a)], we need to define the superconducting pair potential in each region. The time-reversal operator interchanges the valleys in a graphene-like bandstructure with pseudospin-1/2, where each valley is represented by a Hamiltonian constructed out of the Pauli matrices. Because of the valley degeneracy, it suffices to consider one of the two possible sets, thus leading to a 4×4 BdG Hamiltonian. Adopting a homogeneous approximation, we follow the construction in Refs. [8, 32] such that the pair potential can be modelled as

$$\Delta(x) = \begin{cases} \Delta_0 e^{i\phi_1} \sigma_0 & \text{for } x < 0 \\ \Delta_0 e^{i(\phi_1 + \phi)} \sigma_0 & \text{for } x > 0 \end{cases}, \quad \sigma_0 = \mathbb{1}_{2 \times 2}, \quad (5)$$

representing BCS-like Cooper pairing in the spin-singlet s-wave channel. The phases of the superconducting order parameter in the two regions are given by ϕ_1 and $\phi_1 + \phi$, such that the phase difference is ϕ . Since the final expressions for the ABSs and the Josephson current depend only on ϕ , we set $\phi_1 = 0$ without any loss of generality. Due to the presence of the Delta function potential barrier between the two superconductors, we need to consider the potential energy function

$$V(x) = V_0 \delta(x). \quad (6)$$

A few important points need to be remembered here in order to contrast our scenario with the linear-in-momentum dispersion cases. Although the thin-barrier limit is equivalent to a Dirac delta potential, we do not have any constraint on the derivatives of the wavefunction across the junctions when the dispersion is linear, implying that the standard delta function potential approximation for thin barriers cannot be taken from the outset [8]. For those situations, we need to start with a finite normal state region (rather than a Dirac delta function), obtain the equations from the boundary conditions at the S-B and B-S junctions, and finally impose the appropriate limits while computing the final solutions [5, 8, 10, 11, 13]. However, for a quadratic dispersion, we can use the Dirac delta approximation from the start because here we have a constraint on the first order derivatives (with respect to the position coordinate along the propagation direction) of the wavefunction across the junction, analogous to the tunneling problem involving a Schrödinger particle.

The BdG Hamiltonian can be constructed as

$$H = \sum_{\mathbf{r}} \Psi^\dagger(\mathbf{r}) H_{\text{BdG}}(\mathbf{r}) \Psi(\mathbf{r}), \quad \Psi(\mathbf{r}) = \begin{bmatrix} c_{A+}(\mathbf{r}) & c_{B+}(\mathbf{r}) & c_{A-}^\dagger(\mathbf{r}) & -c_{B-}^\dagger(\mathbf{r}) \end{bmatrix}^T, \\ H_{\text{BdG}}(\mathbf{r}) = \begin{bmatrix} \mathcal{H}(\mathbf{K} \rightarrow -i\nabla_{\mathbf{r}}) - E_F + V(x) & \Delta(x) \\ \Delta^\dagger(x) & E_F - V(x) - \mathcal{H}(\mathbf{K} \rightarrow -i\nabla_{\mathbf{r}}) \end{bmatrix}, \quad (7)$$

where where $\mathbf{r} = (x, y)$ is the position vector and the indices \pm on the fermionic operators label the two valleys of opposite chiralities.

Here we demarcate the left superconducting region as “L” and the right superconducting region as “R”, with the Delta function barrier being the weak link in the middle. The electron-like and hole-like BdG quasiparticles are obtained from the eigenvalue equation

$$H_{\text{BdG}}(\mathbf{r}) \psi_{\mathbf{K}}(\mathbf{r}) = \varepsilon \psi_{\mathbf{K}}(\mathbf{r}). \quad (8)$$

If $\psi_N(\mathbf{K})$ denotes an eigenfunction of $\mathcal{H}(\mathbf{K})$, then the electronlike and holelike eigenfunctions of $H_{\text{BdG}}(\mathbf{r})$ are given by the expressions [41]

$$\psi_e(\mathbf{K}) = \left[\psi_N(\mathbf{K}) \frac{(\varepsilon - \Omega) e^{-i\varphi}}{\Delta_0} \psi_N(\mathbf{K}) \right] \text{ and } \psi_h(\mathbf{K}) = \left[\psi_N(\mathbf{K}) \frac{(\varepsilon + \Omega) e^{-i\varphi}}{\Delta_0} \psi_N(\mathbf{K}) \right], \quad (9)$$

respectively, where

$$\Omega = i \sqrt{\Delta_0^2 - \varepsilon^2}, \quad (10)$$

and φ represents the phase of the superconducting order parameter.

Let us define the variable

$$\beta = \arccos(\varepsilon/\Delta_0), \quad (11)$$

which will be useful in the expressions that follow. Using Eqs. (4) and (9), let us now spell out the form of the eigen wavefunction

$$\Psi(\mathbf{r}, K_z) = \psi_L(\mathbf{r}, K_z) \Theta(-x) + \psi_R(\mathbf{r}, K_z) \Theta(x), \quad (12)$$

expressed in a piecewise manner for the two regions, setting the chemical potential at $E_F > 0$. We assume that¹ $V_0 \gg E_F \gg \Delta_0$ and $(V_0 - E_F) \gg E_F$. Since the translation symmetry is broken along the x -axis, K_x is not conserved, whereas the transverse momentum component K_z remains unchanged across the junction.

1. In the left superconductor region, we need to construct a linear combination of the form

$$\begin{aligned} \psi_L(\mathbf{r}, K_z) = & a_l \psi_e(-\kappa_x^e, K_z, 0) e^{-i\kappa_x^e x + K_z z} + b_l \psi_h(-\kappa_x^h, K_z, 0) e^{-i\kappa_x^h x + K_z z} \\ & + c_l \psi_e(-\tilde{\kappa}_x^e, K_z, 0) e^{-i\tilde{\kappa}_x^e x + K_z z} + d_l \psi_h(\tilde{\kappa}_x^h, K_z, 0) e^{i\tilde{\kappa}_x^h x + K_z z}, \end{aligned} \quad (13)$$

where

$$\begin{aligned} \psi_e(K_x, K_z, \varphi) & \simeq \begin{bmatrix} e^{i\beta} (E_F + K_z) & e^{i\beta} K_x^2 & e^{-i\varphi} (E_F + K_z) & e^{-i\varphi} K_x^2 \end{bmatrix}^T, \\ \psi_h(K_x, K_z, \varphi) & \simeq \begin{bmatrix} K_z - E_F & K_x^2 & e^{i\beta - i\varphi} (K_z - E_F) & e^{i\beta - i\varphi} K_x^2 \end{bmatrix}^T, \end{aligned} \quad (14)$$

$$\begin{aligned} \kappa_x^e & \simeq k_{\text{mod}} + i\kappa, \quad k_{\text{mod}} \simeq (E_F^2 - K_z^2)^{1/4}, \quad \kappa \simeq \text{Im} \left[\left\{ (E_F + i\Delta_0)^2 - K_z^2 \right\}^{1/4} \right], \\ \kappa_x^h & \simeq -k_{\text{mod}} + i\tilde{\kappa}, \quad \tilde{\kappa} \simeq \text{Im} \left[\left\{ (E_F - i\Delta_0)^2 - K_z^2 \right\}^{1/4} \right], \quad \tilde{\kappa}_x^e = i\kappa_x^e, \quad \tilde{\kappa}_x^h = i\kappa_x^h. \end{aligned} \quad (15)$$

2. In the right superconductor region, the wavefunction localizing at the interface is described by the linear combination (cf. chapter 5 of Ref. [31])

$$\begin{aligned} \psi_L(\mathbf{r}, K_z) = & a_r \psi_e(\kappa_x^e, K_z, \phi) e^{i\kappa_x^e x + K_z z} + b_r \psi_h(\kappa_x^h, K_z, \phi) e^{i\kappa_x^h x + K_z z} \\ & + c_r \psi_e(\tilde{\kappa}_x^e, K_z, \phi) e^{i\tilde{\kappa}_x^e x + K_z z} + d_r \psi_h(-\tilde{\kappa}_x^h, K_z, \phi) e^{-i\tilde{\kappa}_x^h x + K_z z}. \end{aligned} \quad (16)$$

Imposing the continuity of the wavefunction and the constraint on its first order derivatives (with respect to x) across the junction located at $x = 0$, we get the following equations:

$$\psi_L(0, z, K_z) = \psi_R(0, z, K_z) \text{ and } \partial_x \psi_L(x, z, K_z) \Big|_{x=0} - \partial_x \psi_R(x, z, K_z) \Big|_{x=0} = V_0 \psi_L(0, z, K_z). \quad (17)$$

From the four components of the BdG wavefunction, we get $2 \times 4 = 8$ linear homogeneous equations in the 8 unknown variables ($a_l, b_l, c_l, d_l, a_r, b_r, c_r, d_r$), which constitute the coefficients of the piecewise-defined wavefunction. In the resulting equations, the overall x -independent factors of $e^{iK_z z}$ cancel out. Let \mathcal{M} denote the 8×8 matrix constructed out of the coefficients of the 8 variables. For the equations to be consistent, we need to impose the condition $\det \mathcal{M} = 0$. This helps us determine the energy eigenvalues of the subgap ABSs, which are localized near the junction since they decay exponentially with the distance from the weak link into the superconducting region on either side.

¹ The condition $\Delta_0 \ll E_F$ ensures that the mean-field approximation, applicable for using the BdG formalism, is valid. The second condition $(V_0 - E_F) \gg E_F$ arises because we are focussing on the short-barrier regime.

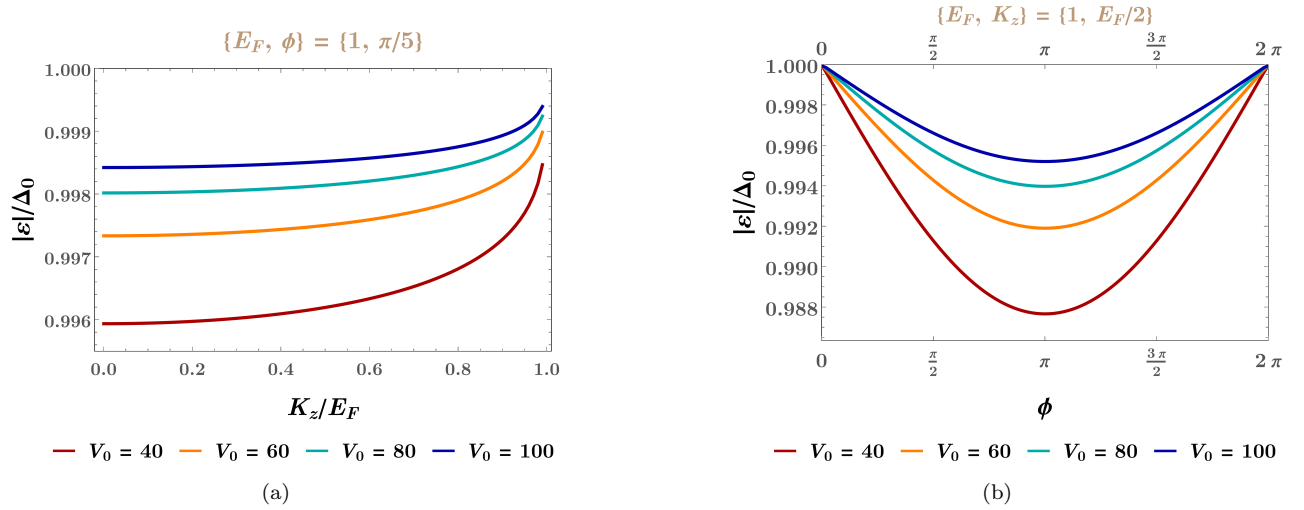


FIG. 2. Behaviour of $|\varepsilon|$ as a function of (a) K_z and (b) ϕ , for some representative values of V_0 (shown in the plot legends), with E_F set to unity.

IV. RESULTS

In order to deal with the determinant of a lower dimensional matrix, we first eliminate four of the eight unknown variables by using four of the linear homogeneous equations. Specifically, in our calculations, we first solve for (a_l, b_l, c_l, d_l) in terms of (a_r, b_r, c_r, d_r) , using $\psi_L(0, z, K_z) = \psi_R(0, z, K_z)$. These solutions are plugged in the constraint $\partial_x \psi_L(x, z, K_z)|_{x=0} - \partial_x \psi_R(x, z, K_z)|_{x=0} = V_0 \psi_L(0, z, K_z)$, such that (a_l, b_l, c_l, d_l) no longer appear in the equations resulting from it. Now we construct the 4×4 matrix $\tilde{\mathcal{M}}$ out of the coefficients of the four variables, viz., (a_r, b_r, c_r, d_r) . The consistency condition now reduces to the vanishing of the matrix $\det \tilde{\mathcal{M}} = 0$. The equation resulting from this determinant gives a lower order polynomial equation in $e^{i\beta}$ (compared to the one obtained from $\det \mathcal{M} = 0$) and, hence, is easier to solve. In fact, we obtain a quartic equation in the variable $e^{2i\beta}$.

Employing the steps outlined above, the equation we need to solve reduces to

$$\begin{aligned}
& z^4 (K_z^2 - 25)^2 (V_0 - 2\mathcal{K}_x)^2 (V_0^2 + 4\mathcal{K}_x^2) - 8z^3 (K_z - 5)(K_z + 5)\mathcal{K}_x^2 (\cos \phi - 1)(2\mathcal{K}_x - V_0) [2(K_z^2 - 25)\mathcal{K}_x - V_0 K_z^2] \\
& + 16z^2 \mathcal{K}_x^2 \sin^2\left(\frac{\phi}{2}\right) [V_0^2 K_z^2 (K_z^2 - 25) - 2V_0(2K_z^4 - 75K_z^2 + 625)\mathcal{K}_x + \{4(K_z^2 - 50)K_z^2 + 3750\}\mathcal{K}_x^2 - 1250\mathcal{K}_x^2 \cos \phi] \\
& + 40000\mathcal{K}_x^4 \sin^4\left(\frac{\phi}{2}\right) + 80000z\mathcal{K}_x^4 \sin^4\left(\frac{\phi}{2}\right) = 0,
\end{aligned} \tag{18}$$

where $z = 1 + e^{2i\beta}$. The order of the polynomial equation (whose roots we need to determine) is the same as what is found for the case of the linearly dispersing Rarita-Schwinger-Weyl (RSW) semimetal, featuring four bands (rather than two), which was analysed in Ref. [13].

The coefficients of various powers of z in Eq. (18) are all real and hence we can analyze the nature of the roots by applying the general criteria applicable for a real quartic polynomial equation. First we obtain the associated depressed quartic, which takes the form $z^4 + qz^2 + \rho z + \gamma = 0$. Let d be the discriminant. For a given set of values for E_F , V_0 , and K_z , we compute numerically the values of d , q , and γ . For each case, we find that $d > 0$ for admissible values of E_F , V_0 , and K_z . This means that if $q > 0$ or $4\gamma - q^2 > 0$, we get a pair of complex conjugate roots. This is what we find from our numerical simulations. However, since $z = 1 + e^{2i\beta}$, as an admissible solution must satisfy the condition $|z - 1| = 1$. From our numerical data, we find that only one of the pair of complex conjugate roots fall in the allowed category. This is in contrast with the RSW case [13], where we get, in general, four distinct solutions for $|\varepsilon|$.

From the above analysis, we arrive at the conclusion that the energies of the subgap states appear as the pairs $\pm|\varepsilon|$ for a doubly degenerate value of $|\varepsilon|$. Therefore, for each value of $|\varepsilon|$, we get a total of four ABSs — two with the value $|\varepsilon|$ and two with the value $-|\varepsilon|$. To demonstrate the results, we include some representative plots, and all of these are obtained by setting $E_F = 1$. In Fig. 2, we show the behaviour of $|\varepsilon|$ as a function of (a) K_z (with a fixed value of ϕ), and (b) ϕ (with a fixed value of K_z), for some representative values of V_0 . The bound state energies are periodic in ϕ with period 2π . They are, in fact, functions of $\cos \phi$, as is evident from Eq. (18). This dependence is reflected in the nature of the curves in Fig. 2(b). Fig. 3(a) illustrates the variation of $|\varepsilon|$ -values against the ϕ - K_z plane and, hence, shows the dependence of the bound state energies on both these variables in a combined way.

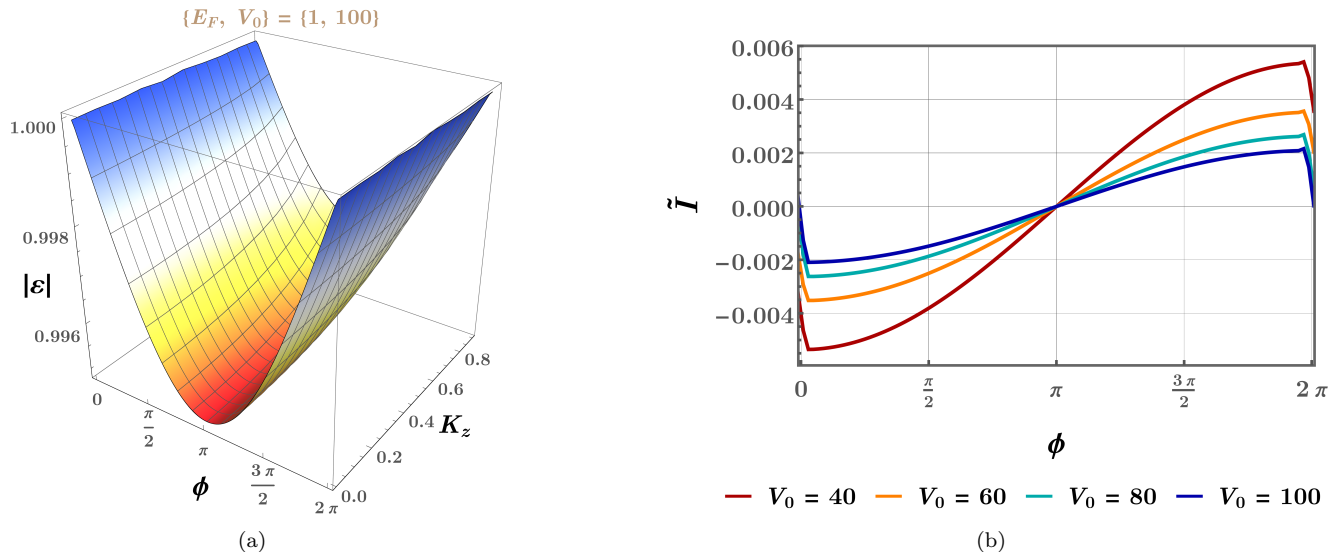


FIG. 3. (a) Magnitude of the energy ε of the Andreev bound states against the ϕ - K_z plane for $E_F = 1$ and $V_0 = 100$. (b) The behaviour of the total Josephson current ($\propto \tilde{I}$), in arbitrary units, as a function of ϕ , obtained at $E_F = 1$ and $k_B T = 0.005 \Delta_0$. We have used four values of V_0 as shown in the plot legends.

The Josephson current density across the junction at a temperature T is given by [5, 6]

$$I_J(\phi) = -\frac{2e}{\hbar} \frac{W}{2\pi} \sum_{n=1}^4 \int dK_z \frac{\partial \varepsilon_n}{\partial \phi} f(\varepsilon_n), \quad (19)$$

where ε_n labels the energy values of the four Andreev bound states and $f(\zeta) = 1/(1 + e^{\zeta/k_B T})$ is the Fermi-Dirac distribution. Fig. 3(b) shows the behaviour of I_J as a function of ϕ , scaled by appropriate numbers/variables (this scaled quantity being denoted as \tilde{I}), for four values of V_0 .

V. SUMMARY AND OUTLOOK

In this paper, we have computed the characteristics of the emergent ABSs, and the resulting Josephson current, in a Josephson junction built with a two-dimensional semi-Dirac semimetal. The junction is taken to be perpendicular to the quadratically dispersing direction in this anisotropic material, featuring hybrid dispersion. The weak link between the two superconducting phases is modelled by a Dirac delta function potential. Using the BdG formalism, we have determined the wavefunction localizing at the junction for $|\varepsilon| \ll \Delta_0$. This requires a piecewise continuous definition — the usual procedure for solving reflection and transmission problems in quantum mechanics involving junction configurations. Demanding consistency of the equations obtained from matching the boundary conditions at the junction, we arrive at a quartic polynomial equation in an appropriate variable (related to the modulus of the ABS energy ε), obtained from the vanishing of the relevant determinant. The physically admissible roots of this quartic give the discrete energy spectrum ε of the ABSs. Although a closed form solution cannot be found due to the fourth order polynomial involved, we have deduced the nature of the roots from our numerical data. We have found that the values of $|\varepsilon|$ are doubly degenerate, leading to four ABSs — two with energy $|\varepsilon|$ and two with energy $-|\varepsilon|$. We have also shown that the solutions depend on the phase difference (ϕ) between the two superconducting regions via functions of $\cos \phi$.

Our main finding is that, because of the quadratic dispersion, we need to include the “evanescent” wave solutions while defining the wavefunctions in each region. This is stark with the cases where the propagation axis is along a direction of linear-in-momentum dispersion [5, 8, 10–13]. The existence of the extra solutions results in a higher order polynomial equation to be solved, compared to the analogous linearly dispersing cases [5, 8, 10–12] with the same number of bands involved. In fact, comparing our results with the isotropic four-band RSW system studied earlier [13], the order of the polynomial for propagation along the quadratic-in-momentum dispersion in a two-band system is the same as that in a linearly dispersing four-band system.

In future, it will be worthwhile to study the Josephson effect in 3d multi-Weyl semimetals [11, 12, 39, 40], by considering the Josephson junction aligned perpendicular to one of the nonlinearly dispersing directions. Another interesting avenue is to introduce a tilt in the Hamiltonian [12] and investigate the resulting ABSs. Last but not the least, analysis of Josephson junctions built with isotropic Luttinger semimetals harbouring quadratic band crossing points [42, 43] is left for future

work.

-
- [1] B. D. Josephson, Coupled Superconductors, *Rev. Mod. Phys.* **36**, 216 (1964).
- [2] K. K. Likharev, Superconducting weak links, *Rev. Mod. Phys.* **51**, 101 (1979).
- [3] J. R. Waldram, The Josephson effects in weakly coupled superconductors, *Reports on Progress in Physics* **39**, 751 (1976).
- [4] C. W. J. Beenakker and H. van Houten, The Superconducting Quantum Point Contact, in *Nanostructures and Mesoscopic Systems*, edited by W. P. Kirk and M. A. Reed (Academic Press, 1992) pp. 481–497.
- [5] M. Titov and C. W. J. Beenakker, Josephson effect in ballistic graphene, *Phys. Rev. B* **74**, 041401 (2006).
- [6] A. Zagoskin, *Quantum Theory of Many-Body Systems: Techniques and Applications*, Graduate Texts in Physics (Springer International Publishing, 2016).
- [7] D. Bolmatov and C.-Y. Mou, Josephson effect in graphene SNS junction with a single localized defect, *Physica B: Condensed Matter* **405**, 2896 (2010).
- [8] M. Maiti and K. Sengupta, Josephson effect in graphene superconductor/barrier/superconductor junctions: Oscillatory behavior of the Josephson current, *Phys. Rev. B* **76**, 054513 (2007).
- [9] K. A. Madsen, E. J. Bergholtz, and P. W. Brouwer, Josephson effect in a Weyl SNS junction, *Phys. Rev. B* **95**, 064511 (2017).
- [10] U. Khanna, D. K. Mukherjee, A. Kundu, and S. Rao, Chiral nodes and oscillations in the Josephson current in Weyl semimetals, *Phys. Rev. B* **93**, 121409 (2016).
- [11] K. Kulikov, D. Sinha, Y. M. Shukrinov, and K. Sengupta, Josephson junctions of Weyl and multi-Weyl semimetals, *Phys. Rev. B* **101**, 075110 (2020).
- [12] D. Sinha, Josephson effect in type-I Weyl semimetals, *Phys. Rev. B* **102**, 085144 (2020).
- [13] I. Mandal, Andreev bound states in superconductor-barrier-superconductor junctions of Rarita-Schwinger-Weyl semimetals, arXiv e-prints (2023), [arXiv:2312.16164](https://arxiv.org/abs/2312.16164) [cond-mat.supr-con].
- [14] M. D. Bachmann, N. Nair, F. Flicker, R. Ilan, T. Meng, N. J. Ghimire, E. D. Bauer, F. Ronning, J. G. Analytis, and P. J. W. Moll, Inducing superconductivity in Weyl semimetal microstructures by selective ion sputtering, *Science Advances* **3**, e1602983 (2017).
- [15] P. Dietl, F. Piéchon, and G. Montambaux, New magnetic field dependence of Landau levels in a graphenelike structure, *Phys. Rev. Lett.* **100**, 236405 (2008).
- [16] S. Banerjee, R. R. P. Singh, V. Pardo, and W. E. Pickett, Tight-binding modeling and low-energy behavior of the semi-Dirac point, *Phys. Rev. Lett.* **103**, 016402 (2009).
- [17] S. Banerjee and W. E. Pickett, Phenomenology of a semi-Dirac semi-Weyl semimetal, *Phys. Rev. B* **86**, 075124 (2012).
- [18] V. Pardo and W. E. Pickett, Half-metallic semi-Dirac-point generated by quantum confinement in TiO₂/VO₂ nanostructures, *Phys. Rev. Lett.* **102**, 166803 (2009).
- [19] V. Pardo and W. E. Pickett, Metal-insulator transition through a semi-Dirac point in oxide nanostructures: VO₂ (001) layers confined within TiO₂, *Phys. Rev. B* **81**, 035111 (2010).
- [20] A. Kobayashi, Y. Suzumura, F. Piéchon, and G. Montambaux, Emergence of Dirac electron pair in the charge-ordered state of the organic conductor α -(BEDT-TTF)₂I₃, *Phys. Rev. B* **84**, 075450 (2011).
- [21] Y. Suzumura, T. Morinari, and F. Piéchon, Mechanism of Dirac point in α type organic conductor under pressure, *Journal of the Physical Society of Japan* **82**, 023708 (2013).
- [22] Y. Hasegawa, R. Konno, H. Nakano, and M. Kohmoto, Zero modes of tight-binding electrons on the honeycomb lattice, *Phys. Rev. B* **74**, 033413 (2006).
- [23] P. Adroguer, D. Carpentier, G. Montambaux, and E. Orignac, Diffusion of Dirac fermions across a topological merging transition in two dimensions, *Phys. Rev. B* **93**, 125113 (2016).
- [24] G. Montambaux, F. Piéchon, J.-N. Fuchs, and M. O. Goerbig, Merging of Dirac points in a two-dimensional crystal, *Phys. Rev. B* **80**, 153412 (2009).
- [25] G. Montambaux, F. Piéchon, J.-N. Fuchs, and M. O. Goerbig, A universal Hamiltonian for motion and merging of Dirac points in a two-dimensional crystal, *The European Physical Journal B* **72**, 509 (2009).
- [26] P. Delplace and G. Montambaux, Semi-Dirac point in the Hofstadter spectrum, *Phys. Rev. B* **82**, 035438 (2010).
- [27] I. Mandal and K. Saha, Thermopower in an anisotropic two-dimensional Weyl semimetal, *Phys. Rev. B* **101**, 045101 (2020).
- [28] S. Sekh and I. Mandal, Circular dichroism as a probe for topology in three-dimensional semimetals, *Phys. Rev. B* **105**, 235403 (2022).
- [29] I. Mandal and K. Saha, Thermoelectric response in two-dimensional nodal-point semimetals, arXiv e-prints (2023), [arXiv:2309.10763](https://arxiv.org/abs/2309.10763) [cond-mat.mes-hall].
- [30] H. J. Kwon, K. Sengupta, and V. M. Yakovenko, Fractional ac Josephson effect in p- and d-wave superconductors, *European Physical Journal B* **37**, 349 (2004).
- [31] Y. Asano, *Andreev Reflection in Superconducting Junctions*, SpringerBriefs in Physics (Springer Nature Singapore, 2021).
- [32] C. W. J. Beenakker, Specular Andreev reflection in graphene, *Phys. Rev. Lett.* **97**, 067007 (2006).
- [33] X. Feng, Y. Liu, Z.-M. Yu, Z. Ma, L. K. Ang, Y. S. Ang, and S. A. Yang, Super-Andreev reflection and longitudinal shift of pseudospin-1 fermions, *Phys. Rev. B* **101**, 235417 (2020).
- [34] W. Chen, L. Jiang, R. Shen, L. Sheng, B. G. Wang, and D. Y. Xing, Specular Andreev reflection in inversion-symmetric Weyl semimetals, *Europhysics Letters* **103**, 27006 (2013).
- [35] S. Uchida, T. Habe, and Y. Asano, Andreev reflection in Weyl semimetals, *Journal of the Physical Society of Japan* **83**, 064711 (2014).
- [36] S.-B. Zhang, F. Dolcini, D. Breunig, and B. Trauzettel, Appearance of the universal value e^2/h of the zero-bias conductance in a Weyl semimetal-superconductor junction, *Phys. Rev. B* **97**, 041116 (2018).

- [37] P. V. Sriluckshmy, K. Saha, and R. Moessner, Interplay between topology and disorder in a two-dimensional semi-Dirac material, *Phys. Rev. B* **97**, 024204 (2018).
- [38] D. A. Khokhlov, A. L. Rakhmanov, and A. V. Rozhkov, Scattering on a rectangular potential barrier in nodal-line Weyl semimetals, *Phys. Rev. B* **97**, 235418 (2018).
- [39] Y.-H. Deng, H.-F. Lü, S.-S. Ke, Y. Guo, and H.-W. Zhang, Quantum tunneling through a rectangular barrier in multi-Weyl semimetals, *Phys. Rev. B* **101**, 085410 (2020).
- [40] I. Mandal and A. Sen, Tunneling of multi-Weyl semimetals through a potential barrier under the influence of magnetic fields, *Physics Letters A* **399**, 127293 (2021).
- [41] C. Timm, Theory of Superconductivity: Lecture Notes (2020-2023).
- [42] I. Boettcher and I. F. Herbut, Superconducting quantum criticality in three-dimensional Luttinger semimetals, *Phys. Rev. B* **93**, 205138 (2016).
- [43] I. Mandal, Fate of superconductivity in three-dimensional disordered Luttinger semimetals, *Annals of Physics* **392**, 179 (2018).